Developmental Cell
Article

A Mec1- and PP4-Dependent Checkpoint Couples Centromere Pairing to Meiotic Recombination

Jill E. Falk,[1] Andrew Chi-ho Chan,[2] Eva Hoffmann,[2] and Andreas Hochwagen[1,*]
[1]Whitehead Institute for Biomedical Research, Cambridge, MA 02142, USA
[2]MRC Genome Damage and Stability Centre, University of Sussex, Falmer BN1 9RQ, UK
*Correspondence: andi@wi.mit.edu
DOI 10.1016/j.devcel.2010.09.006

SUMMARY

The faithful alignment of homologous chromosomes during meiotic prophase requires the coordination of DNA double-strand break (DSB) repair with large-scale chromosome reorganization. Here we identify the phosphatase PP4 (Pph3/Psy2) as a mediator of this process in *Saccharomyces cerevisiae*. In *pp4* mutants, early stages of crossover repair and homology-independent pairing of centromeres are coordinately blocked. We traced the loss of centromere pairing to the persistent phosphorylation of the chromosomal protein Zip1 on serine 75. Zip1-S75 is a consensus site for the ATR-like checkpoint kinase Mec1, and centromere pairing is restored in *mec1* mutants. Importantly, Zip1-S75 phosphorylation does not alter chromosome synapsis or DSB repair, indicating that Mec1 separates centromere pairing from the other functions of Zip1. The centromeric localization and persistent activity of PP4 during meiotic prophase suggest a model whereby Zip1-S75 phosphorylation dynamically destabilizes homology-independent centromere pairing in response to recombination initiation, thereby coupling meiotic chromosome dynamics to DSB repair.

INTRODUCTION

Meiosis is a unique cell division that separates homologous chromosomes (meiosis I) and sister chromatids (meiosis II) to produce the haploid gametes required for sexual reproduction. In most organisms, homologous chromosomes undergo crossover recombination during meiosis. Crossover formation occurs in meiotic G2/prophase by homolog-biased repair of programmed DNA double-strand breaks (DSBs). Repair proceeds through several stable intermediates, including single-end invasions (SEIs) and double-Holliday junctions (dHJs) before resulting in the reciprocal exchange of DNA between homologous chromosomes. In addition to increasing genetic diversity, crossovers provide the physical links between pairs of homologous chromosomes that are necessary for proper chromosome segregation during meiosis I (Bishop and Zickler, 2004).

Characteristic large-scale chromosome movements accompany the individual steps of meiotic DSB repair. Prior to DSB formation, chromosomes undergo a series of homology-independent interactions that are thought to reduce the search space required for homology identification, including the aggregation of telomeres in the "bouquet" conformation (Scherthan, 2001), and the transient assortment of centromeres into nonhomologous pairs (Obeso and Dawson, 2010; Tsubouchi and Roeder, 2005). As DSBs form and promote homology search, the bouquet disperses and nonhomologous centromere pairing is progressively replaced by homologous interactions until, by the time of dHJ formation, homologous chromosomes are aligned along their entire length (Gerton and Hawley, 2005). In most organisms, this alignment is further stabilized by the synaptonemal complex (SC), an elaborate protein lattice that assembles between homologous chromosomes (Page and Hawley, 2004). Following completion of meiotic recombination and disassembly of the SC, centromeres remain paired. At this stage, centromere pairing serves to promote the segregation of nonexchange chromosomes that failed to undergo crossover recombination (Gladstone et al., 2009; Newnham et al., 2010).

How the individual processes of meiotic prophase are temporally coordinated remains poorly understood. Although in some cases coordination may simply be based on metabolic requirements, other observations suggest the existence of regulatory links between prophase events. For example, in budding yeast, the SC component Zip1 is not only required for chromosome synapsis but also promotes crossover formation and is essential for homology-independent centromere pairing (Borner et al., 2004; Sym et al., 1993; Tsubouchi and Roeder, 2005). In addition, a recent study found that the onset of SC assembly at centromeres is actively prevented in the absence of DSB formation, indicating that some prophase events are coordinated by regulatory coupling mechanisms or checkpoints (MacQueen and Roeder, 2009). Because checkpoints by definition create dependent relationships between cell-cycle processes (Hartwell and Weinert, 1989), they are prime candidates for establishing the order of meiotic prophase events.

The DSB-activated checkpoint sensor kinase Mec1 (ATR) is known to have multiple roles in coordinating the response of meiotic cells to programmed DSBs. Mec1 promotes break resection, establishes the homologous chromosome as the preferred meiotic repair template, and delays cell-cycle progression, effectively coupling these processes to meiotic break initiation and repair (Carballo and Cha, 2007; Hochwagen and Amon, 2006). Several meiotic Mec1 targets have been identified, including the chromosomal proteins Hop1 and Mek1, which together help mediate homolog bias (Carballo et al., 2008; Wan et al., 2004), the resection factor Sae2, and the single-stranded

DNA-binding protein RPA (Bartrand et al., 2006; Terasawa et al., 2008). Mec1 signaling through several of these proteins is also critical to delay meiotic cell-cycle progression when break repair or SC formation is defective, a response commonly referred to as the recombination checkpoint or pachytene checkpoint (Hochwagen and Amon, 2006; Roeder and Bailis, 2000). It is important to note, however, that the recombination checkpoint response is only one of several functions of the Mec1-dependent checkpoint machinery in meiotic prophase.

Once meiotic DSBs are repaired, checkpoint targets must be dephosphorylated for meiosis to proceed. In the mitotic DNA damage response, many Mec1-dependent phosphoproteins are substrates of protein phosphatase 4 (PP4), including the checkpoint effector kinase Rad53, RPA, and histone 2A serine 129 (H2A S129), the major DNA damage-dependent chromatin mark (Keogh et al., 2006; Lee et al., 2010; O'Neill et al., 2007). PP4 consists of three subunits, the catalytic subunit Pph3, the coactivator Psy2, and the H2A specificity factor Psy4. Loss of any PP4 subunit in mitotic cells does not cause obvious growth phenotypes, but following DNA damage, mutant cells become trapped in a state of constitutive checkpoint activation because they fail to eliminate Mec1-dependent phosphorylation signals (Keogh et al., 2006; O'Neill et al., 2007).

Here we show that disruption of PP4 also leads to the accumulation of phosphorylated Mec1 targets in meiotic prophase. In this checkpoint-active state, stabilization of single-end invasion intermediates and centromere pairing are blocked, suggesting that these processes are coordinately regulated by PP4. Moreover, we identified Zip1 as the substrate mediating Mec1- and PP4-dependent control of centromere pairing. We found that Zip1 accumulates in a hyperphosphorylated state in *pp4* mutants and identified a single Mec1 consensus site, Zip1 serine 75, as necessary for this modification. Although Zip1 has additional roles in crossover control and SC formation, we found that mutation of serine 75 specifically suppressed the centromere-pairing defect of *pp4* mutants, suggesting that Mec1 efficiently separates the functions of Zip1. Our data demonstrate a role for Mec1 and PP4 in coordinating multiple prophase events in response to DSB formation, and establish a mechanism for the checkpoint control of meiotic centromere pairing.

RESULTS

Persistent Mec1 Signals in the Absence of Pph3 and Psy2

We tested whether PP4 was required to eliminate DSB-dependent checkpoint signals in meiosis. As an initial readout, we monitored the phosphorylation status of two Mec1 substrates, H2A S129 and Rad53, in a synchronous meiotic time course using phospho-specific antibodies and mobility shifts on a western blot. In wild-type cells, phosphorylation of H2A S129 first occurred between 2 and 3 hr after meiotic induction (corresponding to the time of DSB formation) and then disappeared as cells repaired the DSBs and the checkpoint was silenced (Figure 1A). In these cells, Rad53 phosphorylation was barely detectable (Cartagena-Lirola et al., 2008). In *pph3Δ* mutants, by contrast, phosphorylation of H2A S129 and Rad53 accumulated to very high levels and persisted until the end of the time course (Figure 1A). These data indicate that in the absence of PP4, Mec1 signals persist in meiosis.

We wondered whether hyperphosphorylation of H2A and Rad53 was indicative of a recombination checkpoint response. To test this possibility, we compared the phosphorylation patterns of *pph3Δ* mutants with mutants lacking the meiotic repair factors Dmc1 and Hop2. Interestingly, despite the strong recombination checkpoint response triggered by loss of these factors, *dmc1Δ* and *hop2Δ* mutants did not accumulate comparably high levels of H2A and Rad53 phosphorylation (Figure 1A). These data suggest that loss of PP4 does not activate a typical recombination checkpoint response. To further support this notion, we analyzed phosphorylation of Hop1, a well-known meiotic Mec1 target (Carballo et al., 2008). Consistent with previous reports, Hop1 was hyperphosphorylated in *dmc1Δ* and *hop2Δ* mutants (Figure 1A). In contrast, in *pph3Δ* mutants, Hop1 phosphorylation did not accumulate substantially beyond wild-type levels, although it persisted longer than in wild-type cells. Thus, the state of checkpoint activation in *pph3Δ* mutants differs from the canonical recombination checkpoint response to repair defects. Given that meiotic phosphorylation levels of H2A and Rad53 are low in wild-type and even repair-deficient cells, these data suggest that PP4 acts to continuously dephosphorylate a subset of Mec1 targets during meiotic prophase.

To test whether loss of PP4 activity would affect meiotic progression, we analyzed the separation of spindle poles, which marks the end of meiotic prophase. As shown in Figure 1B, spindle pole separation was strongly delayed in the absence of Pph3. Whereas in a wild-type culture spindle poles first separated around 4 hr after meiotic induction (Figure 1B), in *pph3Δ* mutants, spindles only started to accumulate after 7 to 8 hr. We observed similar spindle kinetics when we analyzed mutants lacking Psy2, the other core subunit of PP4 (Figure 1B). Importantly, introduction of a catalytic mutation of the DSB-forming enzyme Spo11 (*spo11-Y135F*) (Keeney et al., 1997) restored almost wild-type kinetics to *pph3Δ* mutants (Figure 1C), indicating that the spindle delay required meiotic DSB formation and was thus likely a consequence of checkpoint activation. The residual delay of *spo11-Y135F pph3Δ* cells (Figure 1C) was due to an earlier role of Pph3 during premeiotic S phase. As shown in Figure S1 available online, premeiotic DNA replication was delayed by approximately 1 hr in the absence of Pph3. This delay was itself Mec1 dependent, because inactivation of Mec1 restored wild-type replication timing to *pph3Δ* mutants (Figure S1). These results are consistent with a role for Pph3 in meiotic S-phase progression, akin to its function in mitotic cells (O'Neill et al., 2007). However, apart from causing a 1 hr delay in DSB formation (see below), this earlier role of PP4 did not interfere with our analysis of PP4 in meiotic prophase.

The delay in spindle formation could be a direct result of persistent Mec1 signaling or a secondary effect of delayed DSB repair. To test whether DSB repair was delayed in *pp4* mutants, we analyzed the kinetics of crossover formation at the well-characterized *HIS4LEU2* recombination hotspot. Engineered restriction site polymorphisms flanking this locus allow the detection of crossover repair products as bands of intermediate sizes between the two parental bands on a Southern blot (Storlazzi et al., 1995). In wild-type cells, DSBs formed approximately 2 hr after meiotic induction and were quickly repaired, as

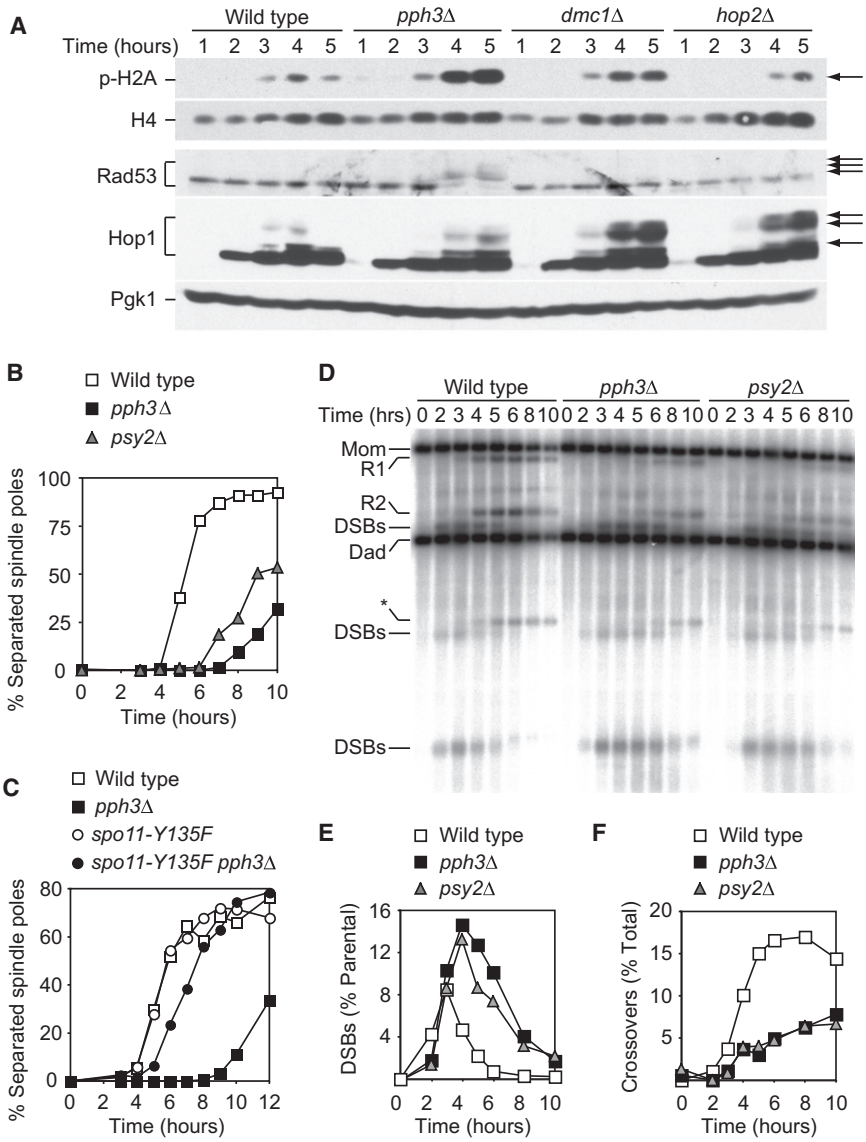

Figure 1. Persistent Mec1 Phosphorylation Marks in the Absence of Pph3 and Psy2

Cultures were induced to undergo synchronous meiosis and samples were taken at the indicated time points.

(A) Western blots of wild-type (A4962), *pph3Δ* (H2086), *dmc1Δ* (H3260), and *hop2Δ* (H5000) cells were probed for phosphorylated H2A S129, and Hop1 and Rad53 protein. Histone H4 and Pgk1 served as loading controls.

(B) Analysis of spindle pole separation in wild-type (A4962), *pph3Δ* (H2086), and *psy2Δ* (H2548) cells by anti-tubulin immunofluorescence.

(C) Spindle analysis of wild-type (A4962), *spo11-Y135F* (H642), *pph3Δ* (H2086), and *pph3Δ spo11-Y135F* (H2118) cells.

(D) Analysis of DSB formation and crossover repair at the *HIS4LEU2* locus in wild-type (NKY1551), *pph3Δ* (H2157), and *psy2Δ* (H3313) strains by Southern blotting. Samples were digested with XhoI and probed with probe A (Storlazzi et al., 1995). R1 and R2 indicate crossover recombinants. The star indicates a meiosis-specific repair product consistently observed at this hotspot (Hunter and Kleckner, 2001).

(E) Quantification of the lower DSB band in (D) as a fraction of the "Mom" signal.

(F) Quantification of the R1 bands in (D) as a fraction of R1 + Mom signal.

See also Figure S1.

indicated by the appearance of crossover repair products starting at around 4 hr (Figure 1D). *pph3Δ* and *psy2Δ* mutants formed DSBs with a slight delay that mirrored the earlier delay in premeiotic DNA replication. Both mutants, however, showed a much longer delay in repairing DSBs, with unrepaired DSBs present at times (6–8 hr) when wild-type cells had already exited meiotic prophase (Figures 1D and 1E). Consistent with this observation, the appearance of crossover repair products was severely delayed, and we observed only a fraction of the crossover levels of wild-type cells in *pph3Δ* and *psy2Δ* mutants by the end of the time course (Figure 1F). Interestingly, despite this block, *pph3Δ* mutants eventually completed meiosis and exhibited only a mild loss in spore viability (Figure S2A), indicating that over time, sufficient crossovers formed in the absence of PP4 to support largely correct meiosis I chromosome segregation. Taken together, these results suggest that the delay in spindle formation is a result of the DSB repair defect of *pp4* mutants.

Early Block to Crossover Formation and Loss of Interference in the Absence of PP4

To determine at what point DSB repair was defective, we analyzed the formation of repair intermediates at the *HIS4LEU2* hotspot. SEI intermediates and dHJs can be stabilized by psoralen interstrand-crosslinking for detection by two-dimensional gel electrophoresis and Southern blotting (Hunter and Kleckner, 2001) (Figures 2A–2C). We found that unresolved dHJs persisted for an extended time in the absence of Pph3, suggesting that PP4 activity is required for the timely resolution of dHJs (Figures 2E and 2F). Interestingly, accumulation of dHJs was only detectable at low temperatures. When *pph3Δ* mutants were incubated at 33°C rather than at 23°C, dHJs failed to form altogether (Figures 2E and 2F). Because SEI levels were also strongly reduced at this temperature (Figure 2D), this observation suggests that Pph3 also promotes an early step in crossover repair. It is worth noting that although absolute levels of dHJs differed strongly, the ratio of interhomolog to intersister dHJs was approximately 4:1 for wild-type and *pph3Δ* cells at both 23°C and 33°C (Figures 2E and 2F), indicating the bias toward repair from the homologous chromosome was maintained in the absence of Pph3. Moreover, unlike crossover repair, noncrossover repair (the homolog-directed repair of DSBs without exchange of flanking sequences) was only mildly defective in *pph3Δ* mutants. In fact, at both temperatures, noncrossovers accumulated beyond wild-type levels in

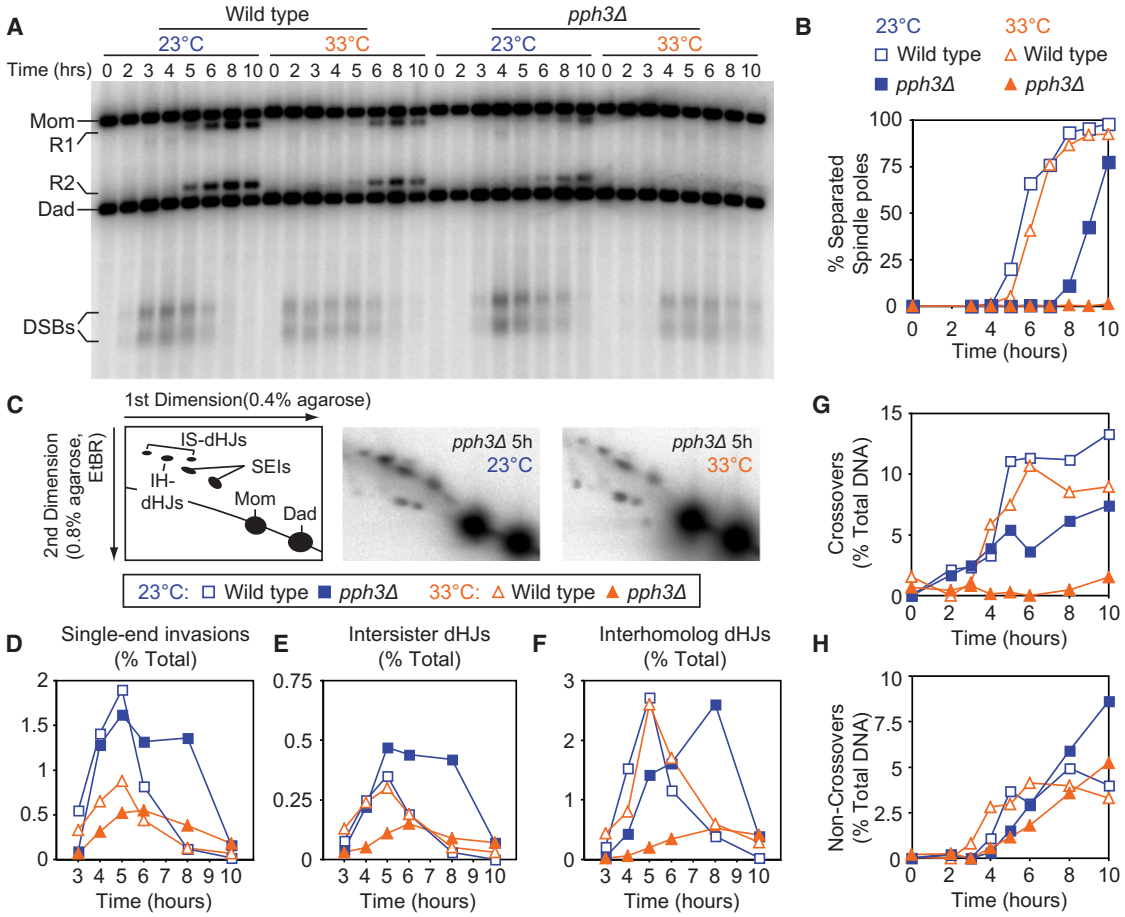

Figure 2. Temperature-Sensitive Crossover Repair Defect

(A–F) Wild-type (NKY3230) and *pph3Δ* (H2530) strains were induced to undergo a synchronous meiosis at 23°C and 33°C. Samples were collected at the indicated time points.

(A) Southern blot of the *HIS4LEU2* locus using an XhoI digest and probe 4 (Hunter and Kleckner, 2001).

(B) Kinetics of spindle formation as determined by tubulin immunofluorescence analysis.

(C) Schematic depicting the positions of single-end invasion and joint molecule (dHJ) intermediates after 2D gel electrophoresis and Southern blotting. Representative blots are shown in the panels to the right.

(D–F) Quantification of SEIs, intersister dHJs (Mom), and interhomolog dHJs. Phosphoimager signals were normalized to a lighter exposure of the Mom spot.

(G and H) Synchronous meiotic time course of wild-type (NKY1551) and *pph3Δ* (H2157) strains analyzed by Southern analysis.

(G) Quantification of crossover products at *HIS4LEU2* (XhoI digest, probe A).

(H) Quantification of noncrossover products (XhoI/MluI digest, probe B) (Storlazzi et al., 1995).

See Figure S2 for schematics of crossover and noncrossover assay systems.

pph3Δ mutants as measured by gene conversion of a restriction site near the DSB site (Figures 2G and 2H). However, their appearance was delayed. Although much of this delay could be attributed to the replication and DSB kinetics of *pph3Δ* mutants, PP4 may, in addition to promoting SEIs, have a minor role in noncrossover repair, in particular at higher temperatures.

We used tetrad analysis to test whether reduced crossover formation in *pph3Δ* mutants was also observed at other loci. Our tester strain carried four genetic markers on chromosomes *III*, *VII*, and *VIII*, demarking three intervals per chromosome (Figure 3). In eight of the nine intervals, the recombination rates were decreased significantly in the *pph3Δ* mutant (Figure 3A; Table S1), indicating that crossover formation is reduced throughout the genome in the absence of Pph3. Furthermore, the crossovers that did form failed to exhibit interference. In wild-type cells, a crossover event typically interferes with the formation of additional nearby crossovers. Interference between genetic intervals can be quantified by calculating crossover frequencies in a given interval grouped by whether or not a crossover occurred in the neighboring interval, and then taking the ratio (Malkova et al., 2004). Thus, a frequency ratio of <1 indicates crossover interference between intervals, whereas the absence of interference yields a ratio of approximately 1. In the wild-type strain, we observed interference among the majority of adjacent intervals (ratios of 0.3–0.6; Figure 3B; Table S1), similar to previous reports (Malkova et al., 2004; Martini et al., 2006). By contrast, in the *pph3Δ* mutant the ratios were overall increased, in many cases to 1 and in some even above 1 (Figure 3B; Table S1). As a result, the ratios were no longer statistically different from the null hypothesis of no interference. These

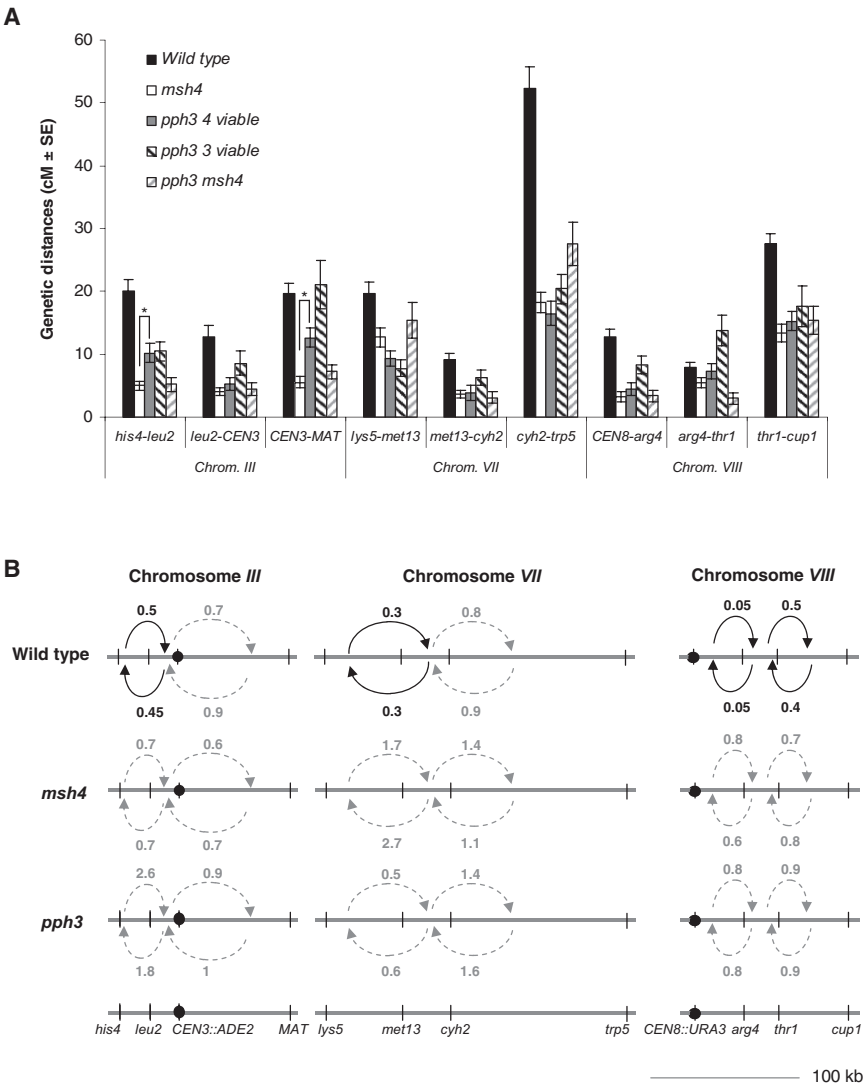

Figure 3. Genetic Analysis of Crossing Over and Crossover Interference in the *pph3Δ* Mutant

(A) Genetic map distances (in centimorgans) of nine genetic intervals on three different chromosomes were analyzed for wild-type (Y1678), *pph3Δ* (Y1675), *msh4Δ* (Y1683), and *pph3Δ msh4Δ* (Y1735) strains. Bars represent the standard error of the mean. All intervals, except *arg4-thr1*, were significantly reduced in the *pph3Δ*, *msh4Δ*, and *pph3Δ msh4Δ* mutants. Stars indicate significant differences between *pph3Δ* and *msh4Δ* ($p < 0.05$, G test for homogeneity).

(B) Crossover interference between a reference and adjacent tester interval. Arrows indicate the effect a crossover has on the map distance of the adjacent interval (see Experimental Procedures). The ratio of the cM values of the tetrads containing a crossover in the reference interval compared to the tetrads without a crossover in the reference interval is given above the arrows. Actual cM distances and further genetic data are given in Table S1. The black arrows represent the presence of interference, whereas gray arrows denote that differences were not statistically significant.

data indicate that interference is significantly reduced or abolished in the absence of PP4.

A temperature-sensitive block in crossover execution combined with a loss of crossover interference is a phenotype that is diagnostic of mutants in the ZMM class of DNA repair factors (Borner et al., 2004; Chen et al., 2008). To test whether the loss of crossover formation and interference of *pph3Δ* cells is comparable to *zmm* mutants, we analyzed the same genetic intervals in a mutant lacking the ZMM factor *MSH4*. As shown in Figure 3, *msh4Δ* cells exhibited a very similar reduction in crossover levels and crossover interference as *pph3Δ* mutants. Moreover, recombination rates of a *pph3Δ msh4Δ* double mutant were no further reduced compared to the single mutants (Figure 3), indicating that *pph3Δ* and *msh4Δ* belong to the same epistasis group for crossover control. It should be noted, however, that these two factors likely also have roles independent of each other in meiosis because the double mutant displayed substantially decreased spore viability compared to the single mutants (Table S1). Taken together, these results suggest that PP4 either functions directly to activate one of the ZMM factors or blocks meiotic prophase immediately prior to ZMM activation. Furthermore, these findings raise the possibility that stabilization of SEIs and the execution of crossover interference are controlled by the Mec1-dependent checkpoint machinery.

Delayed SC Formation and Loss of Centromere Pairing in *pp4* Mutants

Analysis of meiotic chromosome spreads revealed that SC assembly and centromere pairing were also defective in the absence of PP4. We monitored SC morphology by immunofluorescence using an antibody against the SC component Zip1. In wild-type cells, Zip1 initially assembled onto chromosomes in a punctate pattern before forming more extended structures that eventually matured into full SCs (Figure 4A) (Sym et al., 1993). In *pph3Δ* mutants, the initial punctate Zip1 staining occurred with largely wild-type kinetics. However, the Zip1 foci persisted (Figures 4B and 4C), and extrachromosomal Zip1 aggregates (polycomplexes) accumulated to high levels (Figure S3A). Although stretches of continuous SC did eventually form, the staining often retained a beads-on-a-string appearance (Figure 4B). This defect was not caused by an aberrant assembly of meiotic chromosome axes, because Hop1 localization to chromosomes occurred efficiently in the absence of Pph3 (Figure S3B), indicating that loss of PP4 specifically disrupts SC assembly.

In addition to the defect in SC formation, centromere pairing was disrupted in *pph3Δ* mutants. To separate centromere pairing from SC formation, we analyzed meiosis-competent haploid cells expressing both *a* and *alpha* mating-type information

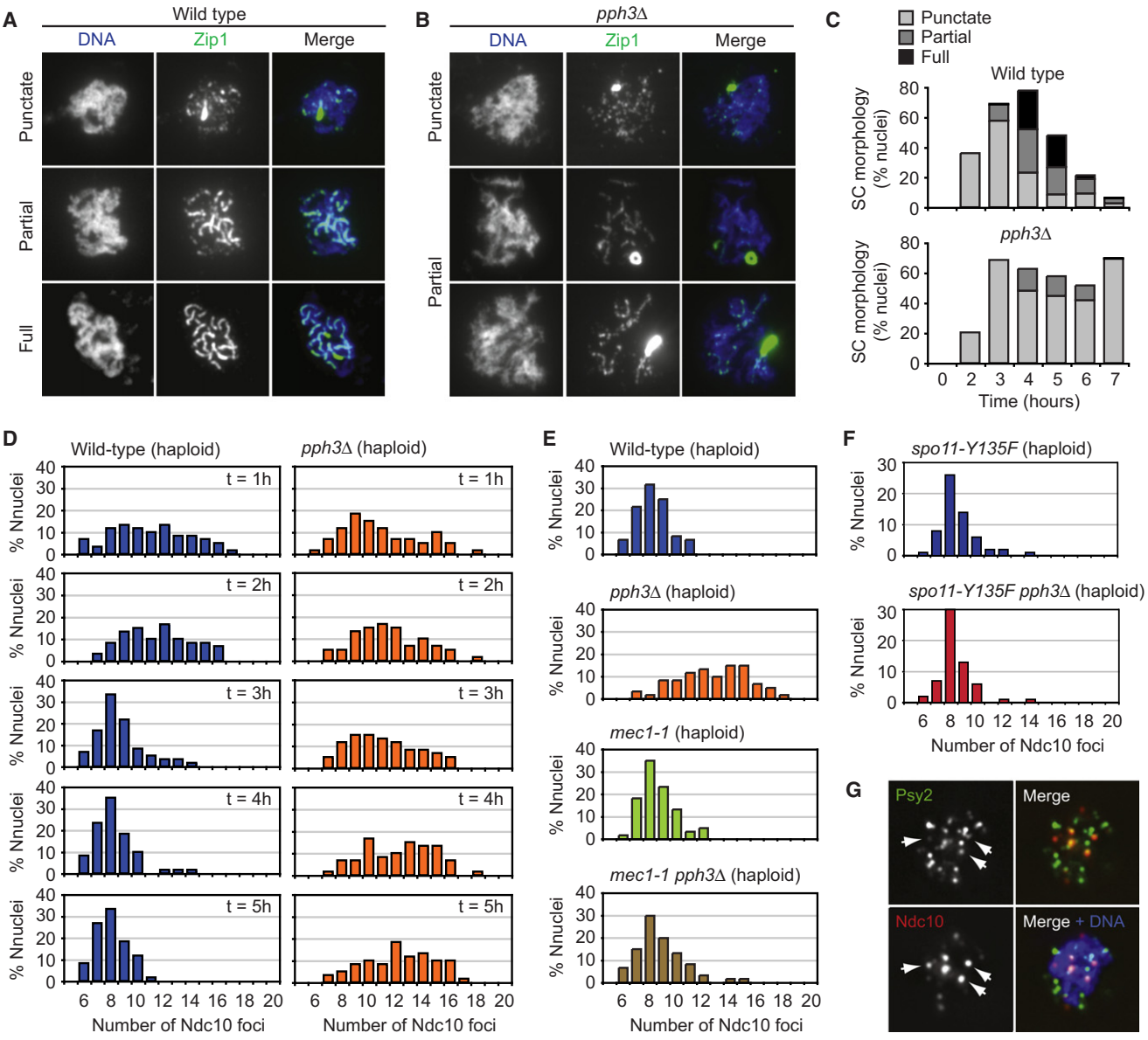

Figure 4. SC Formation and Centromere Pairing Are Blocked in the Absence of PP4

Immunofluorescence analysis of spread meiotic chromosomes.

(A and B) Representative images of Zip1 polymerization in wild-type cells (A4962) and *pph3Δ* mutants (H2086) with Zip1 shown in green and DNA in blue. The bottom panels in (B) show examples of the beads-on-a-string appearance of the SC in *pph3Δ* mutants.

(C) Quantification of Zip1 morphologies of synchronous wild-type and *pph3Δ* cultures.

(D) Wild-type (H4277) and *pph3Δ* (H4255) *MATa/alpha* haploid strains carrying an epitope-tagged Ndc10-6HA construct were induced to undergo synchronous meiosis, and the number of Ndc10 foci on chromosome spreads was determined by immunofluorescence at the indicated time points. Sixty nuclei were counted for each time point. At t = 1 hr, only nuclei that had dispersed from the initial tight clustering of centromeres (Rabl configuration) were counted.

(E and F) Analysis of Ndc10 focus number in *MATa/alpha* haploid checkpoint and DSB mutants. Nuclei were spread 5 and 4 hr after meiotic initiation, respectively, and stained for Ndc10-6HA. Sixty spread nuclei were analyzed for each strain.

(E) Wild-type (H4277), *pph3Δ* (H4255), *mec1-1* (H4568), and *mec1-1 pph3Δ* (H4412).

(F) *spo11-Y135F* (H4189) and *spo11-Y135F pph3Δ* (H4190).

(G) Immunofluorescence analysis of spread wild-type cells (H4069) carrying Psy2-13myc and Ndc10-6HA. Psy2 is shown in green, Ndc10 in red, and DNA in blue. A sampling of three foci that exhibit colocalization between Ndc10 and Psy2 is indicated by arrows.

See also Figure S3.

(Tsubouchi and Roeder, 2005). Although SC formation does occur between nonhomologous chromosomes in *MATa/alpha* haploids (Loidl et al., 1991), it is substantially delayed, whereas homology-independent pairing of centromeres is unaffected in this situation (Tsubouchi and Roeder, 2005). Centromere pairing occurred efficiently in wild-type *MATa/alpha* haploids as

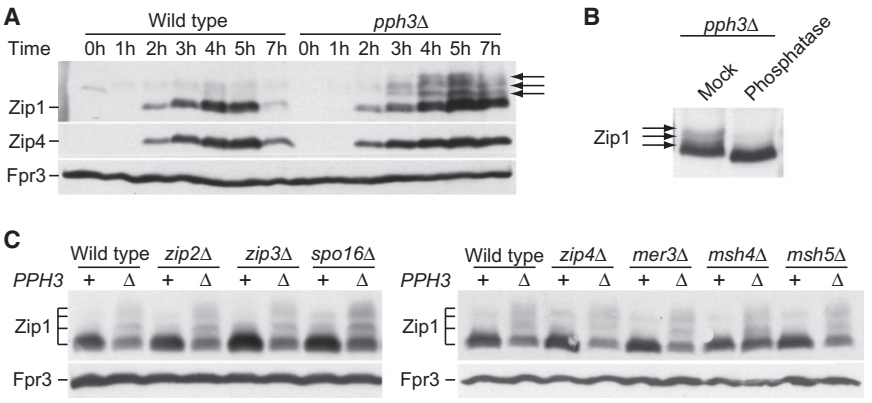

Figure 5. Zip1 Is a Candidate Substrate of PP4

(A) Wild-type (H3206) and *pph3Δ* (H3241) strains carrying a Zip4-6HA construct were induced to undergo a synchronous meiosis. Samples were collected at the indicated time points and analyzed by western blots probed for Zip1 (top panel) and HA (middle panel). Fpr3 was used as a loading control.

(B) Extracts of *pph3Δ* (H2086) cultures 4 hr after meiotic induction were denatured and incubated in alkaline phosphatase buffer with or without alkaline phosphatase, and Zip1 was analyzed by western blotting.

(C) Western blot analysis of Zip1 from meiotic cultures of wild-type (A4962), *pph3Δ* (H2086), *zip2Δ* (H3930), *zip2Δ pph3Δ* (H3993), *zip3Δ* (H3727), *zip3Δ pph3Δ* (H3997), *spo16Δ* (H3957), *spo16 pph3Δ* (H3994), *zip4Δ* (H4176), *zip4Δ pph3Δ* (H4184), *mer3Δ* (H4177), *mer3Δ pph3Δ* (H4178), *msh4Δ* (H4017), *msh4Δ pph3Δ* (H4096), *msh5Δ* (H4070), and *msh5Δ pph3Δ* (H4071), 4 hr after meiotic induction.

See also Figure S4.

assayed by counting the number of foci of the centromere protein Ndc10. The majority of the 16 yeast chromosomes were connected in roughly 8 pairs (9.3 ± 2.5 SD). On the other hand, centromere-pairing efficiency was strongly reduced in *pph3Δ* haploids, as we observed a significant increase in the number of Ndc10 foci (11.5 ± 2.5 SD; $p < 0.001$, Wilcoxon rank-sum test), indicating that PP4 activity is required for efficient centromere pairing in meiosis. The pairing defect became detectable at the time of DSB formation (3 hr), when wild-type haploids exhibited mostly paired centromeres, whereas the centromeres of *pph3Δ* haploids were very frequently unpaired (Figure 4D). Importantly, loss of centromere pairing was the result of checkpoint activation, as centromere pairing was restored by a *mec1-1* mutation (Figure 4E). Consistent with this interpretation, pairing was also restored when DSB formation was prevented using a *spo11-Y135F* mutation (Figure 4F). Finally, we found that Psy2 and Pph3 formed foci on chromosome spreads (Figure 4G; data not shown), indicating that PP4 associates with meiotic chromosomes. A subset of these foci colocalized with Ndc10, suggesting that a pool of PP4 is centromere bound (Figure 4G). Together, these results raise the possibility that PP4 dephosphorylates chromosome-associated substrates to regulate centromere pairing.

Zip1 Is Hyperphosphorylated in the Absence of Pph3 and Psy2

Like PP4, the SC central element component Zip1 is required for the stabilization of single-end invasion intermediates, synapsis, and homology-independent centromere pairing. To test whether Zip1 could be a target of checkpoint signaling, we analyzed the electrophoretic mobility of Zip1 by western blotting. Indeed, several slower-migrating forms of Zip1 became apparent in *pph3Δ* mutants around the time of break formation and persisted at high levels. These forms were also weakly detectable in wild-type cells, but accumulated at much higher levels in *pph3Δ* mutants (Figure 5A). The same increase in Zip1 modification was also observed in a catalytic *pph3-H122N* mutant (Figure S4A) (O'Neill et al., 2007). Consistent with the notion that the mobility shifts were due to persistent phosphorylation, the slower-migrating forms of Zip1 were eliminated upon alkaline phosphatase treatment (Figure 5B). The fact that multiple Zip1 species collapsed into a single faster-migrating band in this experiment furthermore indicates that Zip1 is phosphorylated on multiple residues.

Given that Zip1 is a central component of the SC, we wondered whether Zip1 hyperphosphorylation could be a secondary effect of the SC assembly defect of *pph3Δ* mutants. Because defective SC assembly and polycomplex formation are common phenotypes of *zmm* mutants (Lynn et al., 2007), we analyzed Zip1 phosphorylation in other *zmm* mutants. As shown in Figure 5C and Figure S4B, the hyperphosphorylation of Zip1 was specific to the loss of Pph3 and Psy2. None of the other *zmm* mutants that we tested accumulated the same level of hyperphosphorylated Zip1. Zip1 also did not become hyperphosphorylated in other repair mutants such as *dmc1Δ* or *hop2Δ* (Figure S4C). These results indicate that Zip1 hyperphosphorylation is not a result of defective SC assembly or hyperactivation of the recombination checkpoint. Importantly, hyperphosphorylation of Zip1 in *pp4* mutants also did not depend on any of the known ZMM factors, because Zip1 hyperphosphorylation could be detected in all *pph3Δ zmm* double mutants (Figure 5C). Although it remains a possibility that Zip1 dephosphorylation is mediated by an as yet unknown ZMM factor, the simplest explanation for these data is that Zip1 is a direct target of PP4.

Zip1 Hyperphosphorylation Depends on Mec1

Because all known PP4 substrates in yeast are targets of Mec1, we next tested whether Zip1 hyperphosphorylation required the DSB-dependent activity of Mec1. Consistent with this idea, we found that hyperphosphorylated forms of Zip1 failed to accumulate in DSB-defective *pph3Δ spo11-Y135F* mutants (Figure 6A), indicating that Zip1 hyperphosphorylation requires meiotic DSB formation. When we analyzed Zip1 in *pph3Δ mec1-1* mutants, we found that Zip1 phosphorylation was largely eliminated (Figure 6B), suggesting that Mec1 is required for Zip1 hyperphosphorylation. The loss of Zip1 hyperphosphorylation in *pph3Δ spo11-Y135F* and *pph3Δ mec1-1* mutants was not the result of a premature prophase exit due to the lack of recombination checkpoint activity in these mutants. *pph3Δ spo11-Y135F*

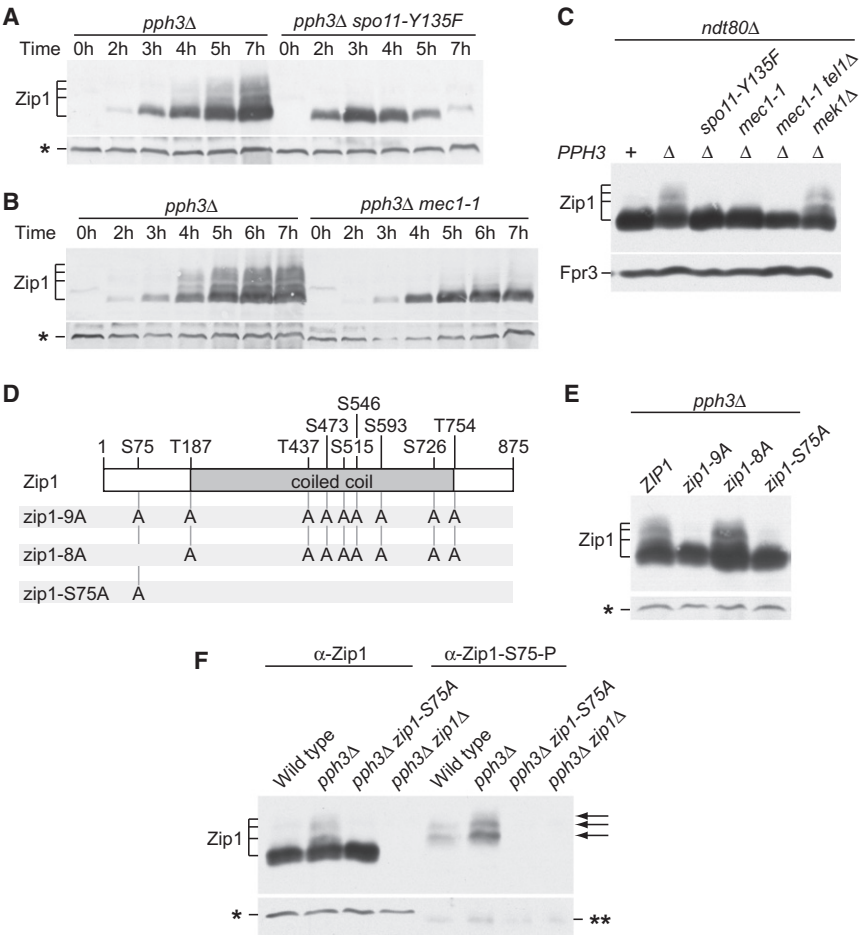

Figure 6. DSB- and Mec1-Dependent Phosphorylation of Zip1

(A) *pph3Δ* (H2086) and *pph3Δ spo11-Y153F* (H2118) strains were induced to undergo a synchronous meiosis. Samples were collected at the indicated time points and analyzed by western blotting for Zip1. A crossreacting band (star) was used as a loading control.

(B) Zip1 analysis of synchronous meiotic cultures of *pph3Δ* (H2086) and *pph3Δ mec1-1 sml1Δ* strains (H2561).

(C) Western blot analysis of Zip1 from cultures 6 hr after meiotic induction of *ndt80Δ* mutants: *ndt80Δ* (H3928), *ndt80Δ pph3Δ* (H3929), *ndt80Δ pph3Δ spo11-Y135F* (H4031), *ndt80Δ pph3Δ mec1-1 sml1Δ* (H4087), *ndt80Δ pph3Δ mec1-1 sml1Δ tel1Δ* (H5010), *ndt80Δ pph3Δ mek1Δ* (H3925). Fpr3 served as a loading control.

(D and E) Analysis of nonphosphorylatable *zip1* mutants.

(D) Schematic indicating the S/TQ consensus sites mutated to AQ in the respective mutants.

(E) Western blot of Zip1 from *pph3Δ* (H4024), *pph3Δ zip1-9A* (H4341), *pph3Δ zip1-8A* (H4181), and *pph3Δ zip1-S75A* (H4462) cultures 4.5 hr after meiotic induction.

(F) Western blots of wild-type (H4025), *pph3Δ* (H4024), *pph3Δ zip1-S75A* (H4462), and *pph3Δ zip1Δ* (H3922) cultures 3.5 hr after meiotic induction were probed for Zip1 and Zip1 serine 75 phosphorylation. Equal amounts of protein were loaded in the left and right halves of the gel. Stars indicate crossreacting bands that served as loading controls.

and *pph3Δ mec1-1* mutants failed to accumulate hyperphosphorylated Zip1 even when prophase exit was prevented by deleting *NDT80*, the transcription factor necessary for exit from meiotic prophase (Figure 6C). To test whether the residual Zip1 shift in *pph3Δ mec1-1* mutants was caused by the Mec1-related kinase Tel1, we deleted *TEL1* in these cells. As shown in Figure 6C, no Zip1 shift could be detected in the *pph3Δ mec1-1 tel1Δ* triple mutant. On the other hand, Zip1 hyperphosphorylation was maintained in the absence of Mek1, the major kinase acting downstream of Mec1 (Figure 6C). These data support the model that Mec1 and Tel1 directly phosphorylate Zip1 independently of Mek1.

Because Mec1 and Tel1 show a strong preference for phosphorylating SQ and TQ sites (Smolka et al., 2007), we analyzed the effect of mutating the serines and threonines of the nine Mec1/Tel1 consensus sites present in Zip1 to alanine. Simultaneous mutation of all S/TQ sites eliminated Zip1 hyperphosphorylation in *pph3Δ* mutants, suggesting that Zip1 is phosphorylated on S/TQ sites (Figures 6D and 6E). Strikingly, a single SQ site in the amino terminus of Zip1 triggers Zip1 hyperphosphorylation. Zip1 hyperphosphorylation was unaffected when the eight S/TQ sites within the coiled-coil region and the C-terminal domain were simultaneously mutated, whereas mutation of serine 75 to alanine abolished Zip1 hyperphosphorylation (Figures 6D and 6E). To confirm that Zip1 serine 75 is indeed phosphorylated, we raised an antibody against a phosphorylated serine 75-containing peptide. As shown in Figure 6F, the phospho-specific antibody specifically detected the higher-migrating forms of Zip1 in *pph3Δ* mutants. Serine 75 phosphorylation could also be detected in wild-type cells, but not in cells in which Zip1 was deleted or serine 75 was mutated to alanine (Figure 6F). These results indicate that Mec1 and Tel1 can phosphorylate Zip1 on serine 75. Phosphorylation of a single site is unlikely to explain the complex phospho-shift pattern of Zip1. Thus, the disappearance of all phosphorylated forms in *zip1-S75A pph3Δ* mutants implies that serine 75 phosphorylation acts as a priming event for further Zip1 hyperphosphorylation, possibly by recruiting a second kinase.

Zip1 Phosphorylation Regulates Meiotic Centromere Coupling

Given that Zip1 is required for crossover repair, synapsis, and centromere pairing, we next tested whether abolishing Zip1 phosphorylation would restore any of these processes to mutants lacking PP4. As shown in Figures 7A and 7B, the *zip1-S75A* mutation did not restore crossover formation in *pph3Δ* mutants (to increase sensitivity, this experiment was conducted at 33°C). Crossover levels were still strongly reduced in the

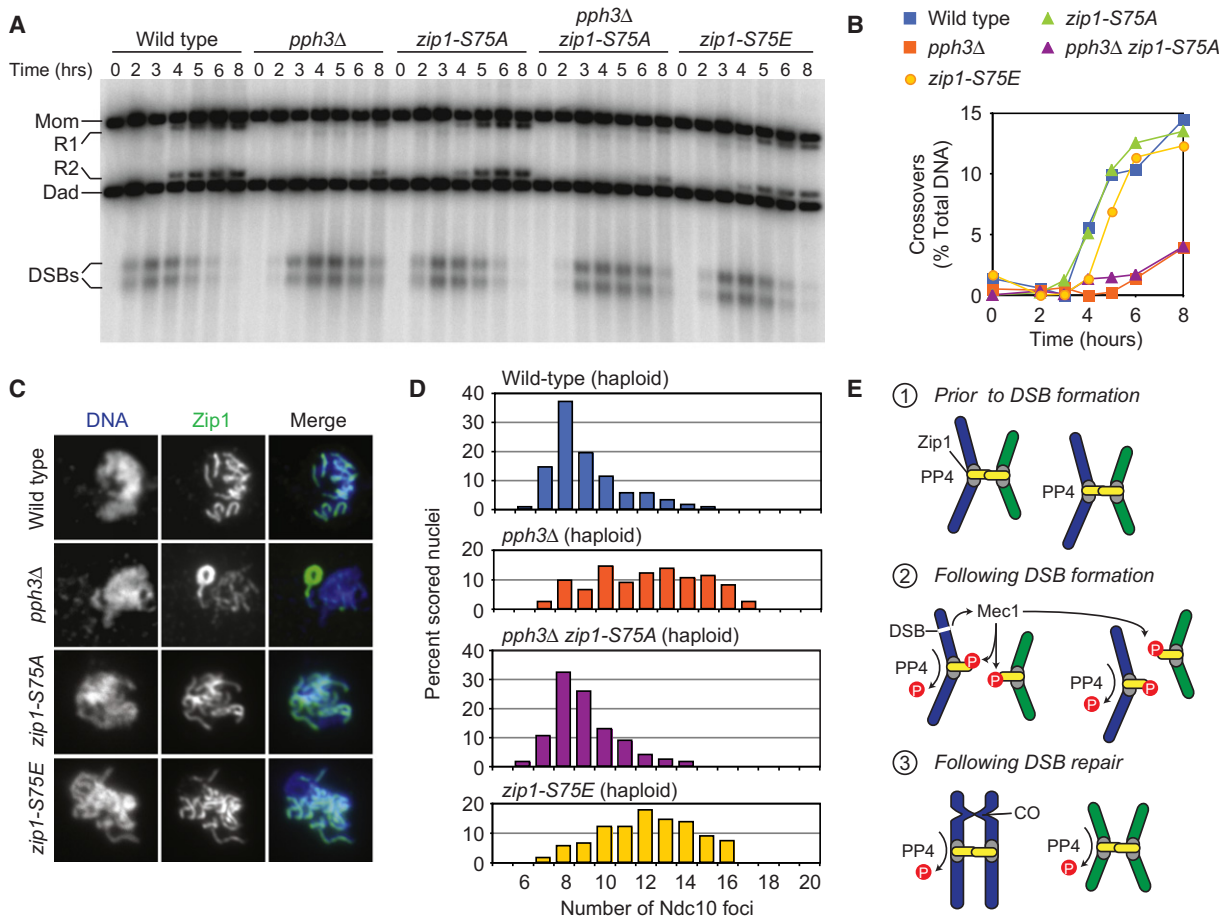

Figure 7. Zip1-S75 Phosphorylation Specifically Controls Centromere Pairing

(A and B) Wild-type (H4446), *pph3Δ* (H4445), *zip1-S75A* (H5207), *zip1-S75A pph3Δ* (H5206), and *zip1-S75E* (H5208) strains were induced to undergo synchronous meiosis at 33°C, and meiotic recombination was monitored at *HIS4LEU2* by Southern blotting (XhoI digest, probe 4) as in Figure 2.

(C) SC formation of wild-type (H4025), *pph3Δ* (H4024), *zip1-S75A* (H5207), and *zip1-S75E* (H5208) strains was analyzed on meiotic spreads by immunofluorescence against Zip1. Zip1 is shown in green and DNA in blue.

(D) Analysis of Ndc10 focus number in *MATa/alpha* haploid wild-type (H4277), *pph3Δ* (H4255), *pph3Δ zip1-S75A* (H4600), and *zip1-S75E* (H4729) cells carrying Ndc10-6HA. Nuclei were spread 4 hr after meiotic initiation and stained for Ndc10-6HA. At least 120 spread nuclei were analyzed for each strain.

(E) Model for the control of centromere pairing by Mec1 and PP4. Blue and green chromosomes represent nonhomologous chromosomes. For simplicity, the sister chromatids of each chromosome are omitted. Gray areas indicate centromeres. Red circles indicate phosphorylation events.

For further description, see Discussion. See also Figure S5.

double mutant, whereas the *zip1-S75A* single mutant formed crossovers with wild-type kinetics. Elimination of all Zip1 S/TQ sites also did not accelerate spindle formation or improve the spore viability of *pph3Δ* mutants (Figures S5A and S5B). Moreover, the *zip1-S75A* mutant exhibited normal synapsis and did not suppress the synapsis defect caused by loss of Pph3 (Figure 7C; data not shown). These data suggest that additional PP4 targets exist that control these processes. Finally, we tested whether preventing Zip1 phosphorylation would restore centromere pairing. As shown in Figure 7D, mutation of serine 75 to alanine restored centromere pairing to *pph3Δ MATa/alpha* haploids (12.1 ± 2.6 versus 9.0 ± 1.6 SD; $p < 0.0001$, Wilcoxon rank-sum test). The pairing of the *pph3Δ zip1-S75A* mutant was not significantly different from wild-type haploids (9.0 ± 1.6 versus 9.0 ± 1.8 SD; $p = 0.399$). Taken together, these results indicate that checkpoint signaling through Mec1 selectively controls one function of Zip1, the homology-independent pairing of centromeres, through phosphorylation of serine 75.

To further test this conclusion, we created a phosphomimetic mutation of Zip1 by replacing serine 75 with a glutamate residue. The *zip1-S75E* mutation did not affect crossover formation, SC assembly, prophase exit, or spore viability (Figures 7A–7C; Figure S5C; data not shown). However, it triggered a Zip1 mobility shift comparable to a *pph3Δ* mutation (Figure S5D). Moreover, consistent with serine 75 controlling centromere pairing, the *zip1-S75E* mutation disrupted centromere pairing in otherwise wild-type *MATa/alpha* haploids (12.1 ± 2.3 versus 9.0 ± 1.8 SD; $p < 0.0001$; Figure 7D). Finally, centromere pairing in this mutant could not be rescued by a *spo11-Y135F* mutation, indicating that the phosphomimetic mutation bypasses the need for checkpoint activation to dissolve centromere pairing (Figure S5E). Together, these results suggest that phosphorylation

of Zip1 serine 75 by the Mec1/Tel1 pathway specifically regulates the centromere-pairing function of Zip1, thereby coupling meiotic chromosome dynamics to DSB repair.

DISCUSSION

Our findings suggest a central role for Mec1-dependent phosphorylation in the control of meiotic prophase. Disruption of the Mec1-counteracting phosphatase PP4 coordinately delayed or blocked several events that are central to meiotic prophase, including the stabilization of SEI intermediates, synapsis, and the nonhomologous pairing of centromeres, and we identified the phosphorylation of Zip1 serine 75 as the mechanism that couples centromere pairing to meiotic DSB repair.

A Role for PP4 in Meiotic Prophase

PP4 is the second checkpoint phosphatase after protein phosphatase 1 (PP1/Glc7) that has been implicated in the control of meiotic prophase. However, the roles of the two phosphatases appear to be markedly separate. PP1 is specifically counteracted by its inhibitor Fpr3 to restrict the timing of PP1 activation to meiotic prophase exit, when it dephosphorylates checkpoint targets to silence the recombination checkpoint and promote cell-cycle progression into metaphase I (Bailis and Roeder, 2000; Hochwagen et al., 2005). By contrast, PP4 appears to be highly active throughout meiotic prophase. We found that even in situations of strong checkpoint activation, such as *dmc1Δ* mutants, the phosphorylation levels of the PP4 targets H2A and Rad53 remained low, whereas they increased dramatically in the absence of PP4. These observations suggest that during meiotic prophase in wild-type cells, PP4 targets are continuously but transiently phosphorylated. If these phosphorylation events alter the activity of protein targets, as we observed for Zip1, such dynamic phosphorylation could provide a mechanism to rapidly modulate protein activity as meiotic prophase progresses.

Checkpoint Control of Centromere Pairing

Our observation that centromere pairing is sensitive to DSB formation raises the question of why such crosstalk between chromosome dynamics and DSB repair would be necessary. One reason may lie in the fact that the initial pairing of centromeres by Zip1 occurs independently of homology (Tsubouchi and Roeder, 2005), but that Zip1 later functions to connect and correctly orient centromeres in meiosis I (Gladstone et al., 2009; Newnham et al., 2010). Thus, at some point during meiotic prophase, the initial nonhomologous associations must be eliminated to correctly pair homologous chromosomes. We propose that the phosphorylation of Zip1 mediated by Mec1/Tel1 allows for this switch. In this model, DSB formation leads to the Mec1-dependent phosphorylation of Zip1 serine 75, which weakens or dissolves the linkages between nonhomologous centromeres (Figure 7E). Because PP4 localizes to centromeres, centromeric Zip1 phosphorylation may only occur transiently before being removed by PP4. Consistent with this possibility, centromeres are predominantly paired during prophase (Tsubouchi and Roeder, 2005), suggesting that loss of centromere pairing is short lived. However, such transient instability of linkage may be sufficient to support the switch to the homologous pairing of centromeres.

In addition, this model could explain how Zip1 helps to specifically segregate nonexchange chromosomes that failed to undergo crossover formation (Gladstone et al., 2009; Newnham et al., 2010). As homologous chromosome pairs align, recombine, and become stabilized by the SC, the centromeres of exchange chromosomes would be eliminated from the pool of centromeres that are available for homology-independent pairing (Kemp et al., 2004). Thus, by a process of exclusion, nonexchange chromosomes would remain as the only chromosomes available for homology-independent linkage by Zip1 (Figure 7E). Importantly, checkpoint signaling would allow stabilization of centromere pairing only once all DSBs are processed. In this way, it would maximize the time for DSB-dependent homology search until homology-independent centromere pairing remains as the only way to connect chromosomes for segregation.

Control of the Zip1 Pairing Function

Several effects could contribute to the loss of centromere pairing by Zip1 serine 75 phosphorylation. The amino-terminal globular domain of Zip1 that harbors serine 75 forms part of the central interface between synapsed chromosomes (Dong and Roeder, 2000). Moreover, it lies immediately adjacent to the coiled-coil regions that mediate the Zip1-Zip1 bridging interactions (Tung and Roeder, 1998). In the simplest model, electrostatic repulsion of phosphorylated serine(s) 75 may serve to weaken these Zip1 head-to-head interactions, thereby disrupting interchromosome bridging and centromere pairing. However, our observation that *zip1-S75E* mutants exhibit normal SCs argues against this possibility. In fact, the amino-terminal globular domain of Zip1 is dispensable for SC formation (Tung and Roeder, 1998), which could explain how serine 75 phosphorylation can affect centromere pairing without disrupting the SC. Alternatively, serine 75 phosphorylation may affect the ability of Zip1 to associate with centromeres. However, when we analyzed chromosome spreads of *pph3Δ* mutants, we found Zip1 still localized to centromeres (Figure S5F), which does not support this model. Perhaps the most likely scenario is that serine 75 phosphorylation facilitates recruitment of additional proteins, either by creating a binding site for a phospho-binding protein or by changing the conformation of the amino-terminal domain of Zip1. Indeed, our observation that the S75A mutation eliminates multiple upshifted species of Zip1 suggests that phosphorylation of serine 75 primes Zip1 to be phosphorylated on non-S/TQ sites by a second kinase. The identity of this second Zip1 kinase is currently unknown. Even though both Rad53 and Mek1 harbor phospho-binding domains, deletion of either kinase alone or together failed to eliminate Zip1 hyperphosphorylation (Figure 6E; data not shown). The *Xenopus* homolog of Mec1 was shown previously to act as a priming kinase for polo-like kinase (Yoo et al., 2004), but Zip1 does not harbor consensus polo phosphorylation motifs, and the yeast polo homolog, Cdc5, is only induced after cells exit from meiotic prophase (Sourirajan and Lichten, 2008). Finally, whether the secondary phosphorylation events triggered by serine 75 phosphorylation contribute to the control of centromere pairing or whether they have additional functions will require the identification and mutation of the modified residues.

Other Meiotic Functions of PP4

In addition to centromere pairing, *pp4* mutants are also defective in the stabilization of SEIs, SC assembly, and spindle formation. Of these, SEI stabilization is likely the most immediate process controlled by PP4. Although we cannot exclude the possibility that all three processes are directly regulated by PP4, many *zmm* mutants exhibit delayed spindle formation and defective SC assembly (Lynn et al., 2007), suggesting that the latter problems may be secondary consequences of the SEI stabilization defects. Our data also show that SEI stabilization is controlled independently of Zip1 serine 75 phosphorylation. Thus, this process is mediated by another PP4, and possibly Mec1, target. The identification of a checkpoint substrate that regulates the stabilization of SEIs and interference-dependent crossover repair would be intriguing, because it would indicate that the checkpoint machinery not only responds to but also influences meiotic DSB repair. Perhaps the strongest candidate for such a function is the single-strand-binding protein RPA. RPA is a target of Mec1 and, at least in mitosis, is also dephosphorylated by PP4 (Brush et al., 2001; Lee et al., 2010). Moreover, mutation of an isoform of the RPA1 subunit of RPA leads to specific loss of interference-dependent crossovers in *Arabidopsis* (Osman et al., 2009), and a point mutation in the Rfa2 subunit mimicking constitutive checkpoint phosphorylation alters crossover distributions in yeast (Bartrand et al., 2006). It will therefore be interesting to test whether loss of Rfa2 phosphorylation alleviates the block to SEI formation and crossover execution of *pp4* mutants.

Checkpoint Signaling as a Coupling Mechanism

It should be stressed that checkpoint signaling in the above cases is not a response to an abnormal situation. Rather, the DSBs detected by Mec1/Tel1 are a predictable and essential part of the developmental program of meiotic prophase, and the checkpoint machinery serves as a mechanism to coordinate a metabolically independent process, namely centromere pairing, with DSB repair. Indeed, the ability to establish dependent relationships is an important aspect of the original definition of checkpoints (Hartwell and Weinert, 1989), and our observations indicate that this ability is elegantly exploited in meiosis to establish dependencies and temporal order during meiotic prophase.

Conservation in Other Organisms

Components of the meiotic checkpoint machinery have been implicated in crossover control in other organisms. Mice lacking ATM, one of the homologs of Mec1, exhibit increased levels of crossover formation (Barchi et al., 2008). Moreover, loss of the Mec1 homologs ATM and ATR is associated with strongly increased pairing interactions between nonhomologous chromosomes in plants (Culligan and Britt, 2008). Conversely, RNAi depletion of *pph-4.1*, the catalytic PP4 phosphatase subunit in *Caenorhabditis elegans*, causes elevated levels of univalent chromosomes after meiotic prophase, consistent with a defect in crossover formation (Sumiyoshi et al., 2002). These findings raise the intriguing possibility that the coupling function of the meiotic checkpoint machinery in the control of crossover execution and chromosome dynamics may be a conserved feature of meiotic recombination in most sexually reproducing organisms.

EXPERIMENTAL PROCEDURES

Synchronous Meiosis

Cells were grown for 24 hr in YPD at room temperature, diluted in BYTA (1% yeast extract, 2% tryptone, 1% potassium acetate, 50 mM potassium phthalate) to OD_{600} = 0.3 (OD_{600} = 0.5 for *MATa/alpha* haploids), and grown for another 16 hr at 30°C. Cells were then washed with water and resuspended in SPO (0.3% potassium acetate) at OD_{600} = 1.9 and incubated at 30°C unless otherwise noted.

Two-Dimensional Gel Analysis

Psoralen crosslinking and 2D gel analysis of recombination intermediates were performed as described by Hunter and Kleckner (2001). Briefly, at each time point, 10 ml of meiotic culture was harvested. Cells were resuspended in fresh psoralen buffer (45 mM Tris [pH 8.0], 45 mM EDTA, 10% ethanol, 0.1 mg/ml trioxsalen [Sigma]) and crosslinked with UV light as described in Schwacha and Kleckner (1994). DNA was extracted and digested with XhoI. Samples were separated in the first dimension in 0.4% SeaKem Gold agarose (Lonza)/1× TBE, the gel was stained in 0.5 μg/ml ethidium bromide, and lanes were cut out, rotated, and separated in the second dimension in 0.8% SeaKem LE agarose/1× TBE containing 0.5 μg/ml ethidium bromide. Southern blotting and phosphoimager analysis were performed as described previously (Blitzblau et al., 2007).

Interference Analysis

Diploid strains were sporulated on supplemented potassium acetate plates for 3 days at 30°C. Ascus walls were removed and spores were dissected onto YPD plates. After growth for 3 days at 30°C, spore colonies were replica plated to synthetic complete medium lacking the appropriate nutrient. Crossover interference was determined using the method developed by Malkova et al. (2004). In this method, tetrads are divided into two groups depending upon whether a crossover (tetratype or nonparental ditype) occurred in a given reference interval or not (parental ditype). The frequency of crossover formation in an adjacent interval(s) was then determined and the ratio of the two frequencies (crossover/no crossover) was calculated. For the *pph3Δ* mutant, the crossover data from the four- and three-spore viable tetrads were combined to increase statistical power.

Western Blotting

At the indicated time points, 5 ml of a meiotic culture was harvested, resuspended in 5% trichloroacetic acid (TCA), and incubated on ice for at least 10 min. These samples were then washed in acetone and left to dry overnight. The samples were lysed by bead beating (FastPrep FP120) in TE lysis buffer (10 mM Tris [pH 7.5], 1 mM EDTA, 2.75 mM dithiothreitol). After addition of 3× SDS loading buffer, the sample pH was adjusted to near neutral using 1 M Tris (pH 8.0). For Zip1 phospho-shift analysis, samples were separated on a 150:1 acrylamide-to-bisacrylamide gel. For all other proteins, a ratio of 37.5:1 was used. The Zip1 (y-300) and Rad53 (yC-19) antibodies (Santa Cruz Biotechnology) and the Pgk1 antibody (Invitrogen) were used at a 1:500 dilution. The anti-Hop1 antibody (gift of N. Hollingsworth) was used at 1:5000. HA-tagged Zip4 was detected using a 1:500 dilution of the HA.11 antibody (Covance). Phosphorylated H2A S129 was detected using a phospho-specific antibody (Abcam) at 1:500. The anti-H4 antibody (Abcam) and the anti-Fpr3 antibody (gift of J. Thorner) were used at 1:1000. The anti-Zip1-S75-P antibody (6919PB) was raised against the phosphorylated peptide CKKLITSMSL-pS-QRNHGYS (Covance) and was used at 1:1000.

Meiotic Spreads and Immunofluorescence

Spread meiotic nuclei were prepared using the method of Loidl et al. (1991). Briefly, cells were spheroplasted at 37°C in solution 1 (2% potassium acetate, 0.8% sorbitol, 10 mM dithiothreitol, 130 μg/ml zymolyase 100T [Seikagaku]). Spheroplasting was stopped using ice-cold solution 2 (100 mM MES [pH 6.4], 1 mM EDTA, 0.5 mM $MgCl_2$, 1 M sorbitol). Fifteen microliters of spheroplast suspension was briefly prefixed on a glass slide with 30 μl fixative (4% paraformaldehyde, 3.4% sucrose) and lysed with 60 μl 1% lipsol. After further addition of 60 μl fixative, spheroplasts were spread using a glass rod. Slides were then dried in the fume hood. Slides were blocked with blocking buffer (0.2% gelatine, 0.5% BSA in PBS). Zip1 was detected using the y-300 rabbit

antibody (Santa Cruz Biotechnology) at a 1:100 dilution in blocking buffer and an anti-rabbit FITC antibody (Jackson ImmunoResearch) at 1:200. Ndc10-6HA was visualized using the rat 3F10 anti-HA antibody at 1:100 (Roche Applied Science) and an anti-rat CY3 antibody (Jackson ImmunoResearch) at 1:500. Hop1 was detected using a rabbit antibody (gift of F. Klein) at 1:1000 and the anti-rabbit FITC antibody at 1:100. Psy2-13myc was detected using the mouse 4A6 anti-myc antibody (Millipore) at 1:100 and an anti-mouse FITC antibody (Jackson ImmunoResearch) at 1:100. Images were obtained using a Deltavision microscope and analyzed using softWoRx Explorer 1.3 image analysis software. Immunofluorescence analysis of spindle pole separation was performed as described previously (Hochwagen et al., 2005).

Alkaline Phosphatase Treatment

Cell pellets from a 5 ml meiotic culture were precipitated in 5% TCA, washed with acetone, and dried overnight. Pellets were resuspended in 200 μl alkaline phosphatase buffer (Roche) and 50 μl protease inhibitor cocktail (Sigma) and lysed by bead beating. After diluting lysates with 1.8 ml alkaline phosphatase buffer to neutralize the pH, samples were split in two, and 400 U alkaline phosphatase (Roche) was added to one aliquot. Both aliquots were incubated at 37°C for 30 min before precipitating protein with the addition of 50 μl 100% TCA. Protein pellets were resuspended in 100 μl TE and 3× SDS loading buffer and the pH was adjusted to near neutral using 1 M Tris (pH 8.0) before boiling samples and performing western blot analysis.

SUPPLEMENTAL INFORMATION

Supplemental Information includes five figures, two tables, and Supplemental Experimental Procedures and can be found with this article online at doi:10.1016/j.devcel.2010.09.006.

ACKNOWLEDGMENTS

We are grateful to N. Hunter, S. Roeder, N. Hollingsworth, F. Klein, S. Brill, and A. Desai for sharing strains and reagents for this project and to D. Durocher and F. Klein for sharing unpublished results. We thank G. Bell for help with statistical analyses and B. Joughin, A. Amon, I. Cheeseman, T. Orr-Weaver, and members of the Hochwagen lab for helpful discussions and critical reading of the manuscript. This work was supported in part by research grant 5-FY10-149 from the March of Dimes Foundation and grants from The Stewart Trust and The Smith Family Foundation to A.H.

Received: December 26, 2009
Revised: June 20, 2010
Accepted: August 26, 2010
Published: October 18, 2010

REFERENCES

Bailis, J.M., and Roeder, G.S. (2000). Pachytene exit controlled by reversal of Mek1-dependent phosphorylation. Cell *101*, 211–221.

Barchi, M., Roig, I., Di Giacomo, M., de Rooij, D.G., Keeney, S., and Jasin, M. (2008). ATM promotes the obligate XY crossover and both crossover control and chromosome axis integrity on autosomes. PLoS Genet. *4*, e1000076.

Bartrand, A.J., Iyasu, D., Marinco, S.M., and Brush, G.S. (2006). Evidence of meiotic crossover control in *Saccharomyces cerevisiae* through Mec1-mediated phosphorylation of replication protein A. Genetics *172*, 27–39.

Bishop, D.K., and Zickler, D. (2004). Early decision; meiotic crossover interference prior to stable strand exchange and synapsis. Cell *117*, 9–15.

Blitzblau, H.G., Bell, G.W., Rodriguez, J., Bell, S.P., and Hochwagen, A. (2007). Mapping of meiotic single-stranded DNA reveals double-strand-break hotspots near centromeres and telomeres. Curr. Biol. *17*, 2003–2012.

Borner, G.V., Kleckner, N., and Hunter, N. (2004). Crossover/noncrossover differentiation, synaptonemal complex formation, and regulatory surveillance at the leptotene/zygotene transition of meiosis. Cell *117*, 29–45.

Brush, G.S., Clifford, D.M., Marinco, S.M., and Bartrand, A.J. (2001). Replication protein A is sequentially phosphorylated during meiosis. Nucleic Acids Res. *29*, 4808–4817.

Carballo, J.A., and Cha, R.S. (2007). Meiotic roles of Mec1, a budding yeast homolog of mammalian ATR/ATM. Chromosome Res. *15*, 539–550.

Carballo, J.A., Johnson, A.L., Sedgwick, S.G., and Cha, R.S. (2008). Phosphorylation of the axial element protein Hop1 by Mec1/Tel1 ensures meiotic interhomolog recombination. Cell *132*, 758–770.

Cartagena-Lirola, H., Guerini, I., Manfrini, N., Lucchini, G., and Longhese, M.P. (2008). Role of the *Saccharomyces cerevisiae* Rad53 checkpoint kinase in signaling double-strand breaks during the meiotic cell cycle. Mol. Cell. Biol. *28*, 4480–4493.

Chen, S.Y., Tsubouchi, T., Rockmill, B., Sandler, J.S., Richards, D.R., Vader, G., Hochwagen, A., Roeder, G.S., and Fung, J.C. (2008). Global analysis of the meiotic crossover landscape. Dev. Cell *15*, 401–415.

Culligan, K.M., and Britt, A.B. (2008). Both ATM and ATR promote the efficient and accurate processing of programmed meiotic double-strand breaks. Plant J. *55*, 629–638.

Dong, H., and Roeder, G.S. (2000). Organization of the yeast Zip1 protein within the central region of the synaptonemal complex. J. Cell Biol. *148*, 417–426.

Gerton, J.L., and Hawley, R.S. (2005). Homologous chromosome interactions in meiosis: diversity amidst conservation. Nat. Rev. Genet. *6*, 477–487.

Gladstone, M.N., Obeso, D., Chuong, H., and Dawson, D.S. (2009). The synaptonemal complex protein Zip1 promotes bi-orientation of centromeres at meiosis I. PLoS Genet. *5*, e1000771.

Hartwell, L.H., and Weinert, T.A. (1989). Checkpoints: controls that ensure the order of cell cycle events. Science *246*, 629–634.

Hochwagen, A., and Amon, A. (2006). Checking your breaks: surveillance mechanisms of meiotic recombination. Curr. Biol. *16*, R217–R228.

Hochwagen, A., Tham, W.H., Brar, G.A., and Amon, A. (2005). The FK506 binding protein Fpr3 counteracts protein phosphatase 1 to maintain meiotic recombination checkpoint activity. Cell *122*, 861–873.

Hunter, N., and Kleckner, N. (2001). The single-end invasion: an asymmetric intermediate at the double-strand break to double-Holliday junction transition of meiotic recombination. Cell *106*, 59–70.

Keeney, S., Giroux, C.N., and Kleckner, N. (1997). Meiosis-specific DNA double-strand breaks are catalyzed by Spo11, a member of a widely conserved protein family. Cell *88*, 375–384.

Kemp, B., Boumil, R.M., Stewart, M.N., and Dawson, D.S. (2004). A role for centromere pairing in meiotic chromosome segregation. Genes Dev. *18*, 1946–1951.

Keogh, M.C., Kim, J.A., Downey, M., Fillingham, J., Chowdhury, D., Harrison, J.C., Onishi, M., Datta, N., Galicia, S., Emili, A., et al. (2006). A phosphatase complex that dephosphorylates γH2AX regulates DNA damage checkpoint recovery. Nature *439*, 497–501.

Lee, D.H., Pan, Y., Kanner, S., Sung, P., Borowiec, J.A., and Chowdhury, D. (2010). A PP4 phosphatase complex dephosphorylates RPA2 to facilitate DNA repair via homologous recombination. Nat. Struct. Mol. Biol. *17*, 365–372.

Loidl, J., Nairz, K., and Klein, F. (1991). Meiotic chromosome synapsis in a haploid yeast. Chromosoma *100*, 221–228.

Lynn, A., Soucek, R., and Borner, G.V. (2007). ZMM proteins during meiosis: crossover artists at work. Chromosome Res. *15*, 591–605.

MacQueen, A.J., and Roeder, G.S. (2009). Fpr3 and Zip3 ensure that initiation of meiotic recombination precedes chromosome synapsis in budding yeast. Curr. Biol. *19*, 1519–1526.

Malkova, A., Swanson, J., German, M., McCusker, J.H., Housworth, E.A., Stahl, F.W., and Haber, J.E. (2004). Gene conversion and crossing over along the 405-kb left arm of *Saccharomyces cerevisiae* chromosome VII. Genetics *168*, 49–63.

Martini, E., Diaz, R.L., Hunter, N., and Keeney, S. (2006). Crossover homeostasis in yeast meiosis. Cell *126*, 285–295.

Newnham, L., Jordan, P., Rockmill, B., Roeder, G.S., and Hoffmann, E. (2010). The synaptonemal complex protein Zip1 promotes the segregation of nonexchange chromosomes at meiosis I. Proc. Natl. Acad. Sci. USA *107*, 781–785.

O'Neill, B.M., Szyjka, S.J., Lis, E.T., Bailey, A.O., Yates, J.R., III, Aparicio, O.M., and Romesberg, F.E. (2007). Pph3-Psy2 is a phosphatase complex required for Rad53 dephosphorylation and replication fork restart during recovery from DNA damage. Proc. Natl. Acad. Sci. USA *104*, 9290–9295.

Obeso, D., and Dawson, D.S. (2010). Temporal characterization of homology-independent centromere coupling in meiotic prophase. PLoS One *5*, e10336.

Osman, K., Sanchez-Moran, E., Mann, S.C., Jones, G.H., and Franklin, F.C. (2009). Replication protein A (AtRPA1a) is required for class I crossover formation but is dispensable for meiotic DNA break repair. EMBO J. *28*, 394–404.

Page, S.L., and Hawley, R.S. (2004). The genetics and molecular biology of the synaptonemal complex. Annu. Rev. Cell Dev. Biol. *20*, 525–558.

Roeder, G.S., and Bailis, J.M. (2000). The pachytene checkpoint. Trends Genet. *16*, 395–403.

Scherthan, H. (2001). A bouquet makes ends meet. Nat. Rev. Mol. Cell Biol. *2*, 621–627.

Schwacha, A., and Kleckner, N. (1994). Identification of joint molecules that form frequently between homologs but rarely between sister chromatids during yeast meiosis. Cell *76*, 51–63.

Smolka, M.B., Albuquerque, C.P., Chen, S.H., and Zhou, H. (2007). Proteome-wide identification of in vivo targets of DNA damage checkpoint kinases. Proc. Natl. Acad. Sci. USA *104*, 10364–10369.

Sourirajan, A., and Lichten, M. (2008). Polo-like kinase Cdc5 drives exit from pachytene during budding yeast meiosis. Genes Dev. *22*, 2627–2632.

Storlazzi, A., Xu, L., Cao, L., and Kleckner, N. (1995). Crossover and noncrossover recombination during meiosis: timing and pathway relationships. Proc. Natl. Acad. Sci. USA *92*, 8512–8516.

Sumiyoshi, E., Sugimoto, A., and Yamamoto, M. (2002). Protein phosphatase 4 is required for centrosome maturation in mitosis and sperm meiosis in *C. elegans*. J. Cell Sci. *115*, 1403–1410.

Sym, M., Engebrecht, J.A., and Roeder, G.S. (1993). ZIP1 is a synaptonemal complex protein required for meiotic chromosome synapsis. Cell *72*, 365–378.

Terasawa, M., Ogawa, T., Tsukamoto, Y., and Ogawa, H. (2008). Sae2p phosphorylation is crucial for cooperation with Mre11p for resection of DNA double-strand break ends during meiotic recombination in *Saccharomyces cerevisiae*. Genes Genet. Syst. *83*, 209–217.

Tsubouchi, T., and Roeder, G.S. (2005). A synaptonemal complex protein promotes homology-independent centromere coupling. Science *308*, 870–873.

Tung, K.S., and Roeder, G.S. (1998). Meiotic chromosome morphology and behavior in zip1 mutants of *Saccharomyces cerevisiae*. Genetics *149*, 817–832.

Wan, L., de los Santos, T., Zhang, C., Shokat, K., and Hollingsworth, N.M. (2004). Mek1 kinase activity functions downstream of *RED1* in the regulation of meiotic double strand break repair in budding yeast. Mol. Biol. Cell *15*, 11–23.

Yoo, H.Y., Kumagai, A., Shevchenko, A., and Dunphy, W.G. (2004). Adaptation of a DNA replication checkpoint response depends upon inactivation of Claspin by the Polo-like kinase. Cell *117*, 575–588.